Journal of Materials Chemistry C

Accepted Manuscript

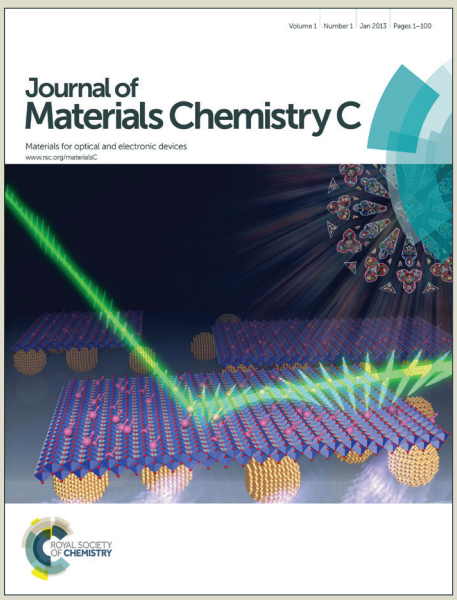

ROYAL SOCIETY OF CHEMISTRY

www.rsc.org/materialsC

Quantum Spin Liquid: Design of a Quantum Spin Liquid next to a Superconducting State based on a Dimer-type ET Mott Insulator

Takaaki Hiramatsu,*[1] Yukihiro Yoshida,[1] Gunzi Saito,*[1] Akihiro Otsuka,[2] Hideki Yamochi,[2] Mitsuhiko Maesato,[3] Yasuhiro Shimizu,[4] Hiroshi Ito,[5] and Hideo Kishida[5]

[1]Department of Agriculture, Meijo University, 1-501 Shiogamaguchi, Tempaku-ku, Nagoya 468-8502, Japan
[2]Research Center for Low Temperature and Materials Sciences, Yoshida-Honmachi, Kyoto University, Sakyo-ku, Kyoto 606-8501, Japan
[3]Division of Chemistry, Graduate School of Science, Kyoto University, Oiwake-cho, Kitashirakawa, Sakyo-ku, Kyoto 606-8502, Japan
[4]Department of Physics, Graduate School of Science, Furo-cho, Chikusa-ku, Nagoya University, Nagoya 464-8602, Japan
[5]Department of Applied Physics, Graduate School of Engineering, Nagoya University, Furo-cho, Chikusa-ku, Nagoya 464-8603, Japan

Abstract

The existence of a spin-disordered quantum state was predicted theoretically by Wannier in 1950 and Anderson in 1973. Various target materials had been considered before the discovery in 2003 of the first quantum spin liquid (QSL) system: a Mott insulator κ-$(ET)_2Cu_2(CN)_3$, where ET is bis(ethylenedithio)tetrathiafulvalene. The family of dimer-type ET conductors κ-$(ET)_2X$ (where X = an anion) exhibits various conduction profiles ranging from insulators to metals to superconductors depending on the counter anion. In κ-$(ET)_2X$, the anion molecules form characteristic patterns of anion openings, on each of which an ET dimer corresponding to a single spin site is positioned, namely a key-keyhole relation. The topological consideration of the crystal structure affords the information on both a spin geometry (t'/t) and electron correlation (U/W), where t and t' are interdimer transfer interactions with an isosceles triangular geometry, and U and W are the on-site Coulomb repulsion energy and bandwidth, respectively. The QSL system κ-$(ET)_2Cu_2(CN)_3$ is characterized by a spin lattice containing nearly equilateral triangles (t'/t = 1.09) with strong electron correlations (U/W = 0.93) at room temperature. The temperature dependences of t'/t and U/W are bases to understand the transport and magnetic behaviors of κ-$(ET)_2X$. κ-$(ET)_2Cu_2(CN)_3$ has a superconducting state next to the QSL state under pressure without passing through an antiferromagnetic state. Here, the design of QSL systems next to a superconducting state is discussed based on the crystal and the electronic structures and physical properties of κ-$(ET)_2X$ using the key-keyhole relation and temperature variant band parameters t, t', U, and W.

1. Introduction: Quantum Spin Liquid State

Except for a 120° compromise lattice,[1] antiferromagnetic (AF) spins cannot be arranged properly in a triangular spin lattice, and strong geometrical spin frustration is produced, as illustrated in Fig. 1a. As a consequence, long-range magnetic ordering is prevented and gives rise to spin-disordered quantum states such as a quantum spin liquid (QSL), as proposed by Anderson.[2] The QSL phase is a quantum-disordered insulating phase, and is assumed to have a ground state containing many degenerate states.[3] To obtain spin frustrated materials, the topology of the spin lattice subject to contradictory constraints is crucial, and the triangular and kagome spin lattices are the main geometries (Fig. 1).[1b,4] However, no QSL systems have

been obtained in strong spin-frustrated materials with a greater spin quantum number ($S > 1/2$), even for triangular or kagome spin lattice topologies, because a system with a high spin quantum number prefers the spin ordered Néel state.[5,6] Furthermore, even for triangular $S = 1/2$ spin systems that have a large AF exchange interaction $|J|$, no such QSL materials have been prepared[5,6] due to the long-standing dearth of guiding principles for QSL materials design.

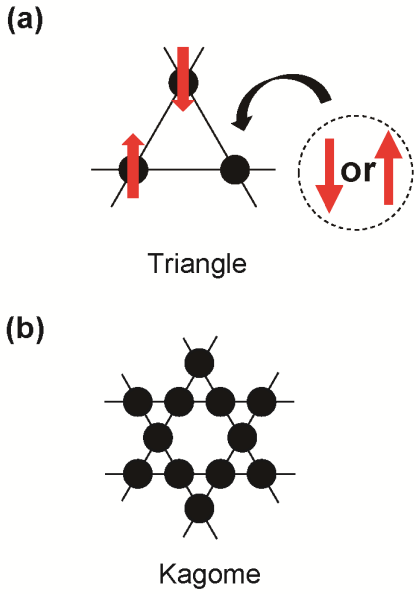

Fig. 1. Geometries of spin lattices exhibiting strong spin frustration: (a) triangle and (b) kagome. The red arrows indicate spins.

The magnetic exchange interaction of spins J is proportional to the square of the transfer interaction t:

$$|J| \sim 4t^2/U, \quad (1)$$

where U is the on-site Coulomb repulsion energy. In a dimer-type conductors such as $(ET)_2X$, where ET is an electron donor: bis(ethylenedithio)tetrathiafulvalene, as illustrated in Fig. 2a, and X is a polymeric or discrete anion (–1), the +1/2 charge of ET molecule provides three-quarter-filled band which splits into upper and lower bands by the dimerization to give a half-filled upper band. A half-filled upper band of κ-$(ET)_2X$ splits at the Fermi level by the on-site Coulomb energy U for the dimer-type Mott insulator. So with decreasing the interdimer distance between two spins (r), a large t, a large bandwidth W, and consequently, a metallic band with itinerant electron forms. Eq. 1 suggests that the QSL state may be near a metallic or superconducting phase in a dimer-type Mott insulator. When the triangular spin lattice is distorted, an AF phase may be preferentially obtained; hence, QSL, AF, and metallic (or superconducting) phases compete with each other depending on t, W, U, J, and other parameters in a dimer-type Mott insulator. The Curie–Weiss temperature Θ_{CW} is a parameter that determines the facility of accessing the QSL state, and is given as

$$\Theta_{CW} = Ng^2\mu_B^2 J(J+1) / 3k_B, \quad (2)$$

where N, g, μ_B, and k_B are the Avogadro number, g-factor, Bohr magneton, and Boltzmann constant, respectively. Therefore, to observe the QSL state at experimentally available temperature, high $|J|$ and $|\Theta_{CW}|$ values are fundamental requirements.

The first QSL system was a charge-transfer (CT) solid of a dimer-type Mott insulator κ-$(ET)_2Cu_2(CN)_3$.[7a] $Cu_2(CN)_3$ is a counter anion (−1 charge), and the ET dimer has both a +1

charge and a spin value of 1/2. The Mott insulator κ-$(ET)_2Cu_2(CN)_3$ has a strong electron correlation, as demonstrated by $U/W = 0.93$, which indicates that the salt is close to the Mott boundary ($U/W \sim 1$).[8] The localized spins on the ET dimers of κ-$(ET)_2Cu_2(CN)_3$ form an equilateral triangular lattice in terms of the interdimer transfer interactions t'/t (= 1.09), as illustrated in Fig. 2c, and the QSL state has been confirmed by nuclear magnetic resonance (NMR), spin susceptibility, and μSR measurements down to 20 mK.[7]

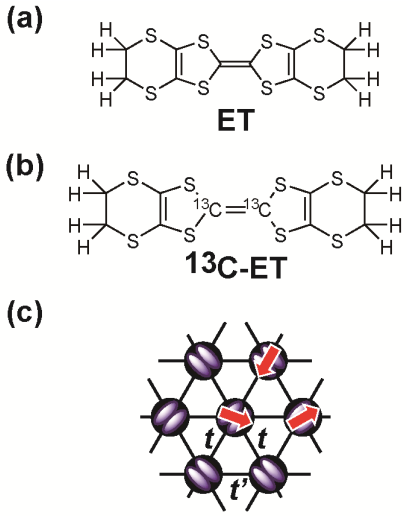

Fig. 2. (a) Diagram of the ET molecule. (b) Diagram of the ^{13}C-ET molecule. (c) Schematic view of the triangular spin lattice of the dimer-type Mott insulator κ-$(ET)_2X$. Blue ellipsoids represent an ET molecule, and black circles represent one spin sites $(ET)_2$. The ratio t'/t represents the shape of the isosceles triangular spin lattice, where the parameters t and t' are inter-dimer transfer interactions. The red arrows indicate spins.

By applying a uniaxial strain to deform the triangular spin lattice of this salt, an anisotropic superconducting state and metallic state was found to appear next to the QSL state without passing through a spin-ordered AF state.[9] This is in marked contrast to the conventional cuprate and C_{60} superconductors, which have AF states next to the superconducting state.[10,11] The insulator–metal transition from the QSL to the metallic state exhibited a positive pressure dependence in the directions of all three crystal axes.[9c] This confirmed the residual spin entropy in the QSL state. ^{13}C NMR measurements under the hydrostatic pressure of the ET salt (with ^{13}C enriched at the central C=C bond), which is presented as ^{13}C-ET in Fig. 2b, indicated both the absence of a Hebel–Slichter peak just below the superconducting critical temperature T_c and a T^3 dependence of the spin-lattice relaxation rate.[12] These facts strongly suggest *d*-wave superconducting symmetry. Thus, the dimer-type Mott insulator κ-$(ET)_2Cu_2(CN)_3$ exhibits competition between the localized (and frustrated), itinerant, and exotic pairing of spins.[7,9,12,13]

Since the discovery of the QSL state in κ-$(ET)_2Cu_2(CN)_3$ (with $|\Theta_{CW}| = 375$ K and $|J|/k_B = 250$ K), several materials based on triangular or kagome lattices have been reported to exhibit such spin states.[4,14] These materials are given as κ-H_3(Cat-EDT-TTF)$_2$ (with a triangular spin lattice, H_2(Cat-EDT-TTF): catechol-fused ethylenedithiotetrathiafulvalene, and $|J|/k_B$ = 80–100 K),[15] the CT solid (ethyltrimethylantimonate)[Pd(dmit)$_2$]$_2$ (with a triangular spin lattice, dmit: 4,5-dimercapto-1,3-dithiole-2-thione, $|\Theta_{CW}|$ = 325–375 K, and $|J|/k_B$ = 220–250 K),[16] $ZnCu_3(OH)_6Cl_2$ (with a kagome spin lattice, $|\Theta_{CW}| = 241$ K, and $|J|/k_B = 170$ K),[17] and $Na_4Ir_3O_8$ (with a hyperkagome spin lattice and $|\Theta_{CW}| = 650$ K).[18] Among these, (ethyltrimethylantimonate)[Pd(dmit)$_2$]$_2$ and $Na_4Ir_3O_8$ exhibit a metallic state

under pressure, but there is no trace of superconductivity. This fact suggests that the interplay is significant between the itinerancy of electrons (metal), pairing of two electrons (superconductor), and localization (Mott insulator, AF, QSL) for the radical electrons on ET dimers in κ-$(ET)_2X$.

In this study, the design of the QSL systems based on the dimer-type Mott insulator κ-$(ET)_2X$ is discussed. Because the main objective of this study is to propose guiding principles of material design for QSLs, the chemical and physical backgrounds of κ-$(ET)_2X$ are described in detail.

2. Dimer-type Mott Insulators κ-$(ET)_2X$: Competition among Itinerancy (Metal, Superconductor), Localization (Mott Insulator), and Frustration (Antiferromagnetic, Quantum Spin Liquid)

2-1. Structural Characteristics and the Key-Keyhole Relation in κ-$(ET)_2X$

The QSL systems to be considered should be studied to very low temperatures ($T < |J|/1000$) using only single crystals of high quality with respect to defects, disorder, impurity, and phase that conceal the intrinsic magnetic nature in many cases, such as $NaTiO_2$.[19] Concerning the issue of temperature, several inorganic QSL candidates, including $NiGa_2S_4$[20] and $Cu_3V_2O_7(OH)_2{\cdot}2H_2O$,[21] suffer from increasing exchange interactions along the weakest direction in the magnetic interactions upon cooling, resulting in magnetic ordering at very low temperatures. In this sense, the two-dimensional (2D) electronic and structural features of κ-$(ET)_2X$ possess advantages for triangular spin lattices as follows.

Characteristic, structural, and physical data of selected $(ET)_2X$ are summarized in Table 1, and are arranged in the order of increasing t'/t. The crystallographic data are given in Tables S1–S7. All the materials listed have a superconducting state at a pressure greater than or equal to ambient pressure. The materials also

Table 1 Transport and magnetic properties, T_c, structural data, and band parameters (t'/t, W, and U/W at room temperature (RT) and 100 K) for CT solids of κ-$(ET)_2X$ arranged in the order of increasing t'/t.

X[a]	space group	L_1, L_2[b]	area of anion layer (RT) (Å^2)	transport behavior[c] σ_{RT} Scm^{-1} (ε_a/meV)	T_c/K (GPa pressurized SC's)	EPR[d] χ_{RT} (10^{-4} emu/mol)	t'/t[e] RT	t'/t[e] 100 K	W[e] RT	W[e] 100 K	U/W[e] RT	U/W[e] 100 K	ground state[f]
a) I_3	$P2_1/c$	Discrete	109.35	good metal, 40–250[#1]	3.6[#1]	no data	0.575	0.541	0.611	0.660	0.800	0.812	SC
b) $Ag(CN)_2{\cdot}H_2O$	$P2_1$	Discrete	108.72	good metal, 27–37[#2]	5.0[#2]	4.0[#3]	0.634	0.609	0.540	0.584	0.884	0.899	SC
c) $Cu(CN)[N(CN)_2]$	$P2_1$	CN, $N(CN)_2$	111.07	good metal*, 5–50	11.2	4.6–4.7	0.690	0.643	0.526	0.553	0.873	0.909	SC
d) $Cu[N(CN)_2]Br$	*Pnma*	$N(CN)_2$, Br	110.78	fuzzy metal, 5–50	11.6[#4]	4.5–5.5	0.672	0.672	0.551	0.593	0.890	0.896	SC[d]
e) $Cu[N(CN)_2]Cl$	*Pnma*	$N(CN)_2$, Cl	109.87	Mott*, 2 (12–52)	12.8 (0.03)[#5]	4.5–5.0	0.715	0.727	0.570	0.607	0.891	0.905	AF[#6](SC)
f) $Cu(NCS)_2$	$P2_1$	SCN, NCS	110.84	fuzzy metal, 5–40	10.4	4.5–5.0	0.880	0.803	0.556	0.555	0.842	0.937	SC[d]
g) $Cu_2(CN)_3$	$P2_1/c$	CN, C/N	114.77	Mott*, 3–7 (42–50)	3.9 (0.06)	5.5	1.091	1.074	0.483	0.480	0.929	1.005	QSL(SC[d])

[a] All data in Table 1 were obtained in our laboratories, except those marked by #1: ref. 22, #2: ref. 23, #3: ref. 24, #4: ref. 25, #5: ref. 26, and #6: ref. 27. [b] The polymerized anions (listed as **c**–**g**) are represented as ML_1L_2, where ligand L_1 links transition metal M^{1+} (Cu^{1+}) to form infinite chains and ligand L_2 attaches to M^{1+} as a pendant or connects the infinite chains. The anion $Ag(CN)_2{\cdot}H_2O$ is either discrete with a dihedral angle for NC–Ag–CN of 156° or has an infinite zigzag chain of –Ag–CN–Ag–CN– where other CN function as pendants. [c] Good metal: the condition where resistivity decreases monotonically down to T_c. Good metal*: the condition where resistivity decreases monotonically down to T_c with a hidden hump at high temperatures. Fuzzy metal: the condition where semiconductive behavior exhibited near RT is followed by metallic and superconducting behaviors. Mott*: the condition where the material becomes a fuzzy metal

and superconductor under pressure (Fig. 5a). [d] EPR: electron paramagnetic resonance. [e] U: on-site Coulomb energy (= $2|t_{b1}|$[13,28]) and W: upper bandwidth. The band parameters [t_{b1}, t_{b2}, t_p, t_q (t_p', t_q' in the case of the crystal with $P2_1$ space group), t, t', U, and W) were calculated using a tight-binding model based on the extended Hückel method using observed crystal structures at RT to 100 K with single-ζ parameters including d-orbitals of sulfur atoms.[29] t' = $|t_{b2}|/2$, t = $(|t_p| + |t_q|)/2$, in the case of the $P2_1$ space group t = $(|t_p| + |t_q| + |t_p'| + |t_q'|)/4$. [f] The ground state under pressure is indicated in parentheses, and the symmetry of the superconductor is shown in square brackets. SC: superconductor, AF: antiferromagnet, and QSL: quantum spin liquid.

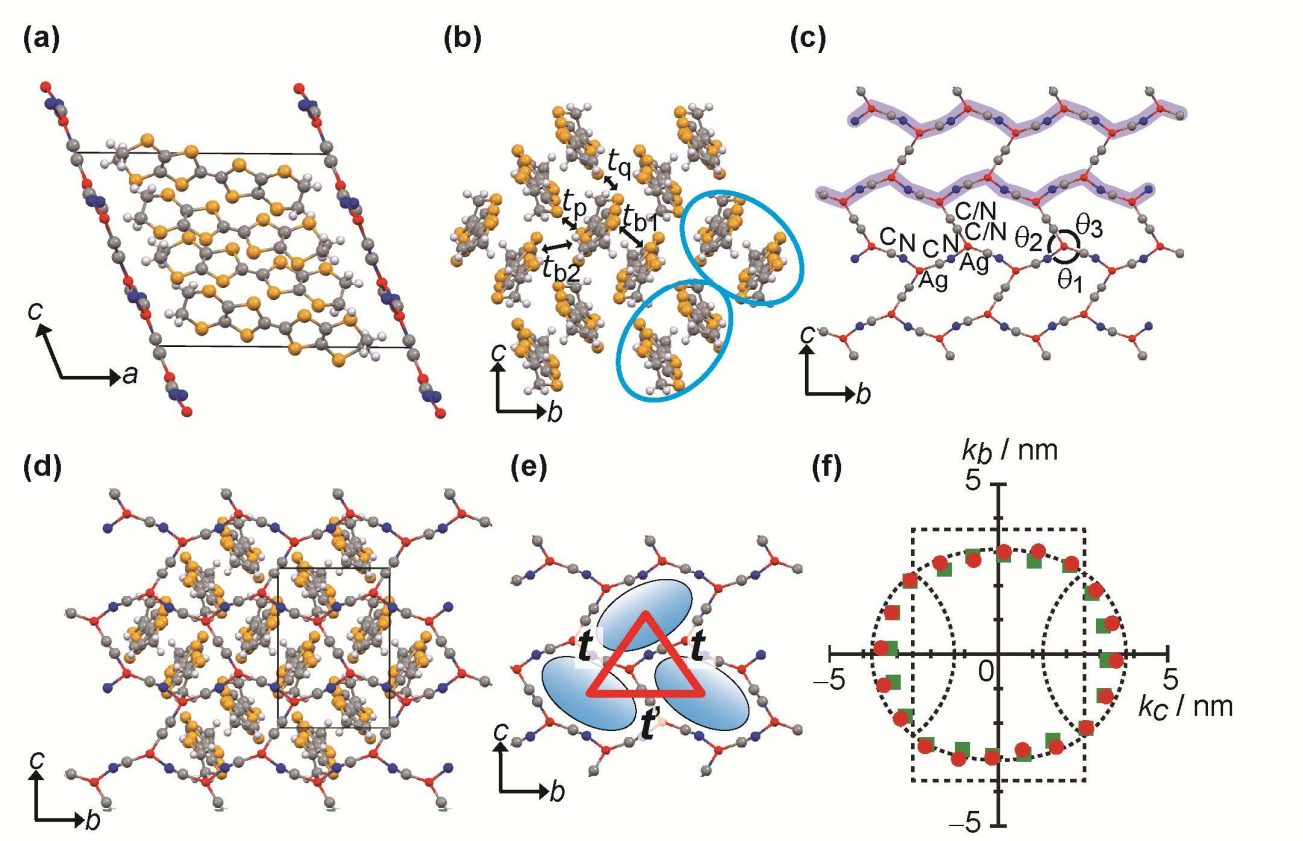

Fig. 3. (a) Crystal structure of κ-$(ET)_2Cu_2(CN)_3$ (listed as material **g** in Table 1) viewed along the b axis at room temperature (RT).[30] The major conformation (79%) of the terminal ethylene groups is depicted, because the terminal ethylene groups were disordered at RT. The color scheme employed is C: gray, S: orange, H: off white, N: blue, and Cu: red. (b) The projected view of ET molecules along the molecular long axis marked with transfer interactions (t_{b1}, t_{b2}, t_p, and t_q). Blue ellipsoids correspond to ET dimers $[(ET^{0.5+})_2]^{1+}$. (c) An illustration of the anion structure. Infinite chains of –Cu–CN–Cu–CN– or –Cu–NC–Cu–NC– along the b axis (two chains are represented by thick blue lines) are connected by disordered CN (indicated by C/N) groups along the c axis to form hexagonal anion openings. The angles θ_1, θ_2, and θ_3 are the dihedral angles around the Cu^{1+} ion. (d) The crystal structure viewed along the a axis obtained by the combination of Figs. (b) and (c). (e) A good correspondence is observed between an ET dimer (1 spin, blue ellipsoid) and the anion opening, indicative of a key(spin)-keyhole(anion opening) relation. The red triangle is the triangle spin lattice with t' = $|t_{b2}|/2$, t = $(|t_p| + |t_q|)/2$. (f) Fermi surface topology of κ-$(ET)_2Cu_2(CN)_3$ determined by the angular dependent magnetoresistance oscillation periods under 0.70 GPa (red circles) and 0.21 GPa (green squares). The dotted lines represent the first Brillouin zone, and the Fermi surface contour was calculated based on the crystal structure at RT and ambient [31]

have very similar donor packing in the crystal. As an example, Figure 3 shows the crystal structure of κ-$(ET)_2Cu_2(CN)_3$. The ET dimers $[(ET^{0.5+})_2]^{1+}$ align orthogonally to each other (Fig. 3b), which is designated as κ-type packing (Fig. 2c), to form a 2D conducting layer in the bc plane. The ET layer is

sandwiched by the insulating anion layers composed of polymerized anions $\{[Cu_2(CN)_3]^{1-}\}_\infty$ along the *a* axis (Fig. 3a).[30] Figure 3b illustrates the important transfer interactions (t_{b1}, t_{b2}, t_p, t_q), and two perpendicularly aligned ET dimers are encircled by blue ellipsoids in the figure. ET molecules align with their terminal ethylene groups directed toward the anion layer (Fig. 3a). Because the electron density of the highest occupied molecular orbital (HOMO) at the terminal ethylene groups of ET molecules is very small, the transfer interactions along the interlayer direction through the anion layer are much smaller than those along the intralayer. Hence, a good 2D nature of the electronic structures of κ-$(ET)_2X$ is maintained down to low temperatures, as confirmed by the Fermi surface topology studies of Shubnikov-de Haas and de Haas-van Alphen, and by angular dependent magnetoresistance oscillations (Fig. 3f).[31,32] For example, the interlayer transfer interaction is less than 1/100 of intralayer one for X = $Cu(NCS)_2$.

The anion $Cu_2(CN)_3$ molecules form a 2D anion network in the *bc* plane (Fig. 3c). The polymerized anions of the salts in Table 1 are represented as ML_1L_2, where ligand L_1 links M^{1+} (= Cu^{1+}) to form infinite chains and ligand L_2 attaches to M^{1+} as a pendant or connects the infinite chains. Two infinite chains composed of Cu^{1+} and CN^{1-}, which is a ligand L_1, is depicted by the thick blue lines in Fig. 3c, and these chains are connected to each other by disordered CN^{1-} (ligand L_2, indicated by C/N). Consequently, the anion $Cu_2(CN)_3$ forms hexagonal anion openings (θ_1 = 118.7 Å, θ_2 = 102.3 Å, and θ_3 = 138.8 Å). The donor and anion layers alternatingly stack along the *a* axis so as to allocate ET dimers (given by the blue ellipsoids in Fig. 3b) on the anion openings shown in Fig. 3c, namely a direct overlap of Fig. 3c on Fig. 3b, giving rise to the crystal depicted in Fig. 3d. Figure 3e is a schematic illustration of Fig. 3d to demonstrate the key-keyhole relation of κ-$(ET)_2Cu_2(CN)_3$, which results in a triangular spin lattice by connecting the centers of the ellipsoids. The key-keyhole relation in ET salts originates from the patterns of the packing motifs between terminal ethylene groups of ET and anion openings.[33]

The calculated Fermi surface of κ-$(ET)_2Cu_2(CN)_3$, shown in Fig. 3f based on the crystal structure at room temperature (RT), is composed of one-dimensional electron-like and 2D cylindrical hole-like Fermi surfaces with no gap between them. Due to the crystal symmetry of κ-$(ET)_2X$, a gap exists between the two types of Fermi surfaces for the salts with $P2_1$ space group **b**, **c**, and **f**, whereas no gap exists for the other materials in Table 1.

2-2. Anion Openings

An anion opening is defined as a region of the anion layer that is unoccupied by anion atoms. Detailed analyses of the crystal structures of ET salts having planar anion layers reveal that the cores of the anion openings correlate with specific hydrogen atom positions of the ET molecule, which are closest to the anion layer within each ethylene group. The pattern of the cores exhibits a 1:1 correspondence with the donor packing motif (α, β, θ, and κ).[33] Therefore, the anion openings in κ-$(ET)_2X$ (for X = $Cu(NCS)_2$ (**f**),[34] $Cu[N(CN)_2]Cl$ (**e**),[26] $Cu[N(CN)_2]Br$ (**d**),[25] $Cu(CN)[N(CN)_2]$ (**c**),[30b-30d] etc.) provide the polyanionic template for ET dimers giving rise to the triangular spin lattice shown in Fig. 2c, which is discussed in detail.

Figures 4a and 4d present schematic figures representative of the crystal structure of the first QSL κ-$(ET)_2Cu_2(CN)_3$ and first 10 K class superconductor κ-$(ET)_2Cu(NCS)_2$, respectively, where the polymerized anion molecules are illustrated by thick 2D walls colored gray, two anion openings are shaded in red, and figurative ET molecules are given in yellow. An ET dimer serves as the spin unit. When the centers of dimerized ET molecules are drawn to occupy and connect the anion openings, the geometrical

pattern composed of an isosceles triangle unit shown in Figs. 4b and 4e is obtained. One kind of isosceles triangle is obtained for κ-$(ET)_2Cu_2(CN)_3$, while two variations of isosceles triangles in terms of interdimer distances (7.86 Å, 7.86 Å, and 8.44 Å) and (7.75 Å, 7.75 Å, and 8.44 Å) are observed for κ-$(ET)_2Cu(NCS)_2$. Using the transfer interactions t (= $(|t_p| + |t_q|)/2$) and t'(= $|t_{b2}|/2$) for κ-$(ET)_2Cu_2(CN)_3$ and averaged transfer interaction $t = (t_1 + t_2)/2$ for κ-$(ET)_2Cu(NCS)_2$ (Fig. 4f), a topological pattern composed of one type of isosceles triangle is obtained as the spin lattice, as illustrated in Fig. 4c.

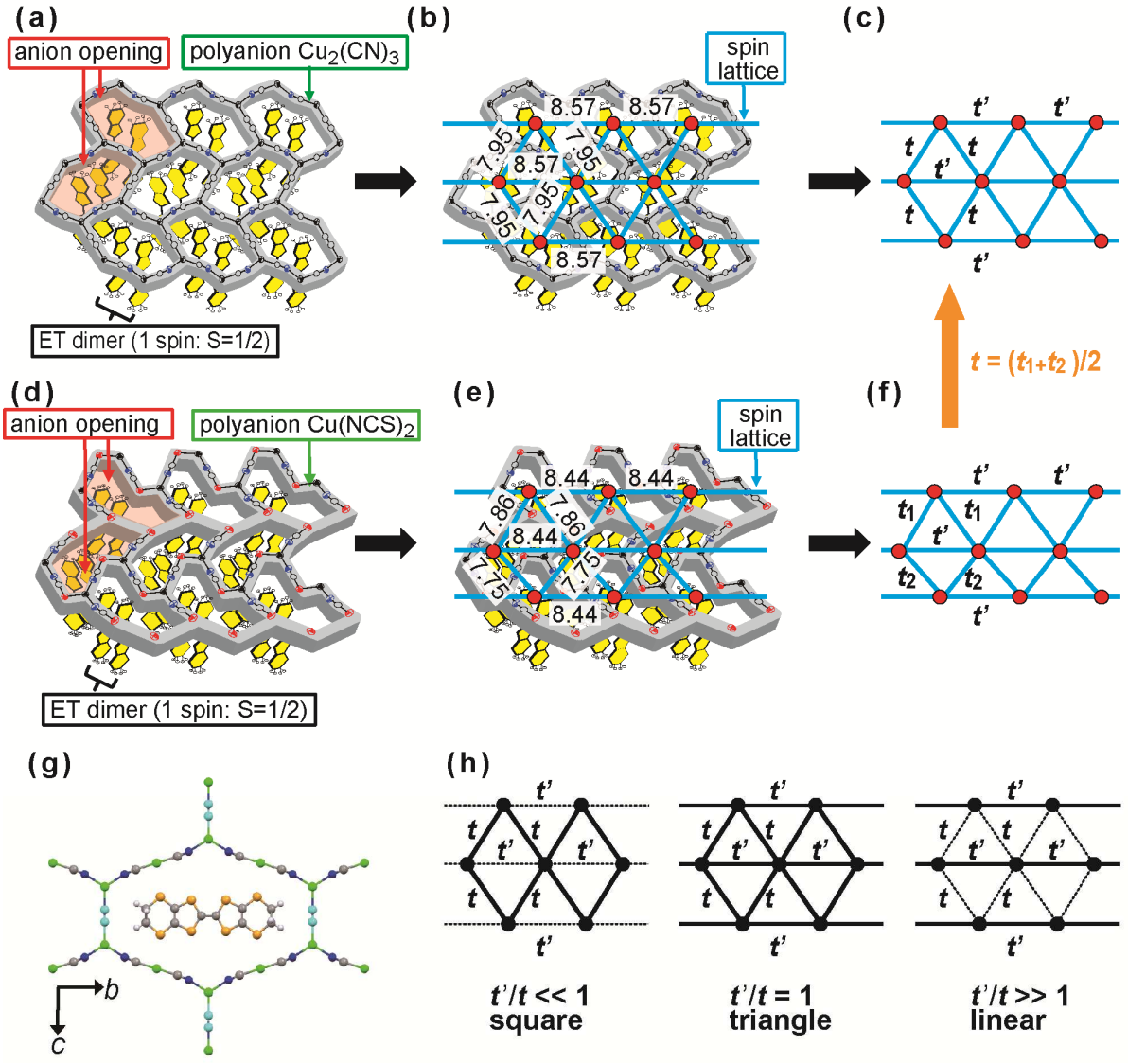

Fig. 4. (a, d) Schematic view of κ-$(ET)_2Cu_2(CN)_3$ (a) and κ-$(ET)_2Cu(NCS)_2$ (d) indicating the $Cu_2(CN)_3$ and $Cu(NCS)_2$ anion structures (represented by black lines on a dark gray thick wall, where Cu: black, S: red, N: blue, and C: white), anion openings (two of which are shaded red), and ET (yellow) single spin dimers. ET dimers are confined to the anion openings. (b, e) The periodic pattern of the anion openings of κ-$(ET)_2Cu_2(CN)_3$ (b) and κ-$(ET)_2Cu(NCS)_2$ (e) represents a two-dimensional (2D) triangular network by connecting centers of ET dimers. The values illustrated indicate the interdimer distances in Å. (c, f) The interdimer transfer interactions form a spin lattice composed of 2D isosceles triangle units. Two kinds of isosceles triangle in κ-$(ET)_2Cu(NCS)_2$ (e, f) is averaged $t = (t_1 + t_2)/2$ to give t'/t value. (g) The crystal structure of $(ET)Ag_4(CN)_5$ viewed along the a axis.[35] The color scheme employed is C: gray, S: orange, Ag: green, N: blue, and disorder C/N: aqua. (h) The spin geometry changes in accordance with changes in t'/t, wherein a 2D square spin lattice for $t'/t \ll 1$, a 2D regular triangle for $t'/t = 1$, and a one-dimensional linear spin lattice is obtained for $t'/t \gg 1$. Stronger and weaker exchange interactions are drawn in solid and dotted lines, respectively.

One of the appropriate parameters to account for the degree of spin frustration is the geometry of the triangle in terms of the intermolecular interactions t'/t. It is expected that an equilateral triangle with $t'/t = 1$ provides maximum spin frustration. The t'/t for QSL system **g** is close to unity at $t'/t = 1.09$, whereas the other κ-type salts have a t'/t less than 0.90 (i.e., **a**–**f**). The Mott insulator κ-$(ET)_2Cu[N(CN)_2]Cl$ has a weak geometrical spin frustration, as indicated by the small $t'/t = 0.72$, and therefore, spins are allowed to form AF spin ordering at 27 K.[27] The interdimer distances (r) and transfer interactions depend on the size and shape of the anion opening, and it is anticipated that salts with larger anion openings have both larger r and smaller interdimer t, resulting in a narrow bandwidth W and a higher density of state at the Fermi level. In fact, the bandwidth W of κ-$(ET)_2X$, as listed in Table 1, decreases with an increasing area of the anion layer, which is defined as the area of the base where the anion molecule resides in a unit cell.

The characteristic features of the 2D triangle network of anion openings of κ-$(ET)_2Cu\mathit{L}_1\mathit{L}_2$ are as follows.

1) The planar tridentate coordination of the Cu^{1+} ions is the main driving force of the triangular spin lattice. Consequently, some transition metal ions having planar tridentate coordination ability, such as Ag^{1+} [36] and Zn^{2+},[37] may also provide for a 2D triangular spin lattice. It is possible that anion species with more than threefold symmetry may also afford such a triangular network of anion openings.
2) Since an anion opening should have an appropriate size and shape to hold one dimer of $ET^{0.5+}$ molecules, the size and shape of the ligands L_1 and L_2 in κ-$(ET)_2M\mathit{L}_1\mathit{L}_2$ are the important parameters for the design of dimer-type ET salts. It is emphasized that a good key-keyhole relation (Figs. 3d, 3e, 4a, and 4d) should be satisfied between ET dimers and anion openings. If the anion opening is very large to hold one ET dimer orthogonally, different types of donor molecules having a larger width may be drawn into the anion opening rather than ET. Otherwise, the ET molecule will fit into the anion opening with a different orientation, such as shown in Fig. 4g for $(ET^{\cdot+})Ag_4(CN)_5$ which has a diamond spin lattice.[35]
3) Depending on the magnitude of the interdimer interaction, the spin lattice will change from a square lattice for $t'/t \ll 1$ to a triangular lattice for $t'/t \sim 1$ and to a linear lattice for $t'/t \gg 1$, as shown in Fig. 4h, where stronger interactions are depicted by solid lines and weaker interactions by dotted lines. Therefore, even if the system is a 2D Mott insulator, the geometrical shape of the spin lattice changes depending on the magnitude of t'/t.

2-3. Competition among Itinerancy (Metal, Superconductor), Localization (Mott insulator), and Frustration (Antiferromagnetic, Quantum Spin Liquid): Mott Boundary and Boundary between Antiferromagnetic and Quantum Spin Liquid States for κ-$(ET)_2X$

The electron correlation of the system is parameterized by U/W, as summarized in Table 1. The transport properties of κ-$(ET)_2X$ exhibit characteristic features depending on the magnitude of U/W, and are accordingly classified into the three groups shown in Fig. 5a.

When U/W is small (**Group A**), the ET salts with X = I_3[22] ($U/W = 0.800$, **a**) and $Ag(CN)_2 \cdot H_2O$[23] ($U/W = 0.884$, **b**) show a simple metallic behavior down to T_c similar to β-$(ET)_2AuI_2$[38a] ($T_c = 4.9$ K, $U/W = 0.837$, **h**). The X = $Cu(CN)[N(CN)_2]$ salt ($U/W = 0.872$, **c**) exhibits a hidden hump near 100 K.[30b]

When U/W is large (≥0.891) (**Group C**), salts with X = Cu[N(CN)$_2$]Cl[26] (U/W = 0.891, **e**) and Cu$_2$(CN)$_3$[30] (U/W = 0.929, **g**) become Mott insulators. The Mott insulator **e** has a small activation energy ε_a for conduction (ε_a = 12 meV > 42 K and 52 meV < 42 K). The other Mott insulator **g** has a much larger activation energy, ε_a = 36–43 meV. **Group C** includes strongly electron-correlated salts.

κ-(ET)$_2$X with an intermediate U/W (**Group B**, where X = Cu[N(CN)$_2$]Br (U/W = 0.890, **d**) and Cu(NCS)$_2$ (U/W = 0.842, **f**)) exhibit semiconductor–metal–superconductor behavior, denoted as a "fuzzy metal." Therefore, salts **a** and **b** are "good metals," and salt **c** resides close to a good metal between a good metal and fuzzy metal.

Even though the U/W values at RT could explain the general tendencies of the transport properties of the various κ-(ET)$_2$X, the values of U/W cannot solely discriminate the three groups, namely 1) the transport behavior of the fuzzy metal **f** suggests that its U/W value (0.842) is larger than those of **b** and **c**, contrary to the calculated U/W values at RT (0.884 for **b** and 0.873 for **c**), and 2) the U/W values at RT of **b**, **c**, **d**, and **e** are very closely located near 0.9. Therefore, it is important to evaluate the temperature dependence of U/W to understand the effect of U/W on the temperature dependence of the resistivity.

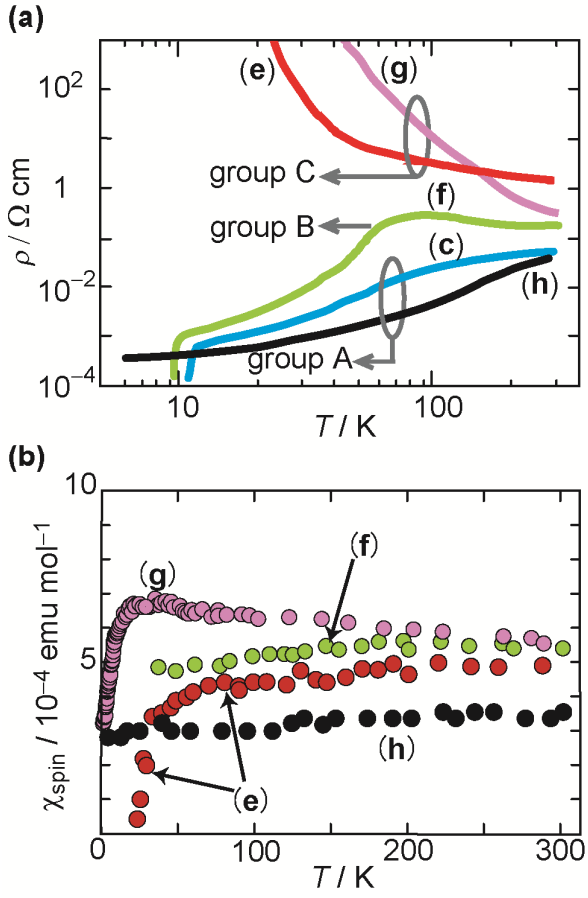

Fig. 5. (a) Typical temperature dependence of the resistivity of three groups of κ-(ET)$_2$X (//2D plane) in Table 1 together with a good metal β-(ET)$_2$AuI$_2$ (**h**). (b) Temperature dependence of spin susceptibility by electron paramagnetic resonance (EPR, single crystals) of **e**, **f**, and **g** in Table 1 together with a good metal β-(ET)$_2$AuI$_2$ (**h**). The data presented were measured in our laboratories, except the χ of salt **h**.[38b]

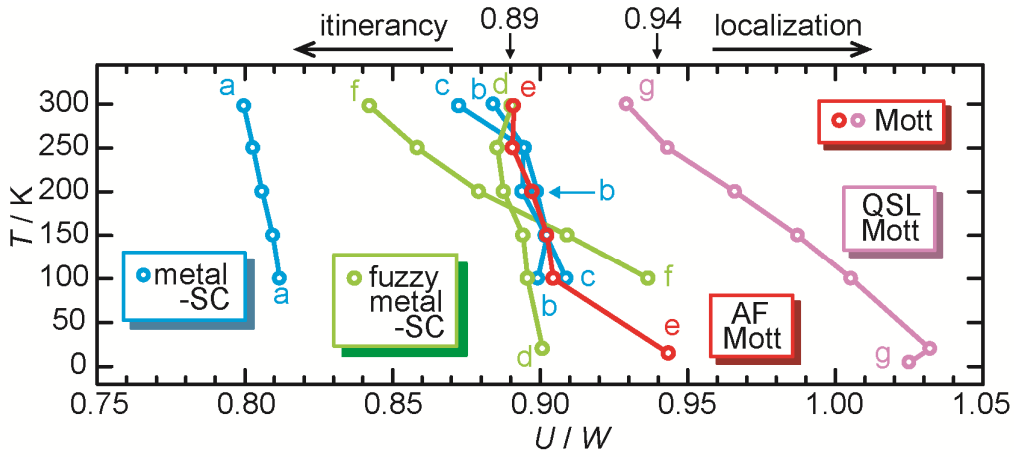

Fig. 6. Temperature dependence of U/W of κ-$(ET)_2X$ (the anions considered are **a**: I_3, **b**: $Ag(CN)_2{\cdot}H_2O$, **c**: $Cu(CN)[N(CN)_2]$, **d**: $Cu[N(CN)_2]Br$, **e**: $Cu[N(CN)_2]Cl$, **f**: $Cu(NCS)_2$, and **g**: $Cu_2(CN)_3$). The low temperature data below 100 K were calculated based on the crystal structures reported by other laboratories for **d**,[39] **e**,[40] and **g**.[41] The color scheme employed is blue symbols: good metal, green symbols: fuzzy metal, red symbols: AF Mott insulator, and magenta symbols: QSL Mott insulator.

As shown in Fig. 6, every salt demonstrated an increase of U/W to some extent with decreasing temperature mainly due to the increase of the dimerization energy $|t_{b1}|$ (= $U/2$). Even though salts **a**–**e** did not show a significant increase of U/W to 100 K (0.7%–4.1% increase), the salts **f** and **g** showed a significant increase of U/W from 8.1% to 11.3%; however, no satisfactory reason for such a diversity in the temperature dependence of U/W can be offered.

Note that the U/W values of the four salts **b**–**e** are nearly equivalent to 100 K, even though their transport properties are quite diverse, namely salts **b** and **c** belong to **Group A**, salts **d** and **f** to **Group B**, and salt **e** to **Group C**. Furthermore, relative to the behavior of salts **b**–**e**, the U/W value of **f** is observed to increase from a much smaller value at RT (0.842) to a larger value at 100 K (0.937), indicating that the electron correlation in this salt was enhanced rapidly with decreasing temperature. At 100 K, the electron correlation of **f** seems much stronger than salt **e** (0.905). The reliable crystallographic data below 100 K derived from other laboratories and included in Fig. 6 show a rapid increase of U/W for **e**[40] and steady increases for **d**[39] and **g**.[41] For **e**, a rapid increase of U/W below 100 K because of the increase of dimerization energy ($2t_{b1} = U$) with almost no change in W is the cause of the formation of the AF phase in this salt.

The information contained in Fig. 6 indicates the following points.

1) According to the observed diversity of the temperature dependence of U/W, it is inappropriate to draw straight vertical lines over the entire temperature range (even 100–0 K), representing a constant U/W has often been depicted in T vs. U/W phase diagrams.[42]
2) The transport property of κ-$(ET)_2X$ is not rationalized by the U/W values at RT, but it must be understood, in part, by the aid of the temperature dependence of U/W.
3) A boundary between localization (Mott insulators **e** and **g**) and itinerancy (metals and fuzzy metals **a**–**d**, and **f**) at low temperature is allocated at around U/W = 0.94, which amounts to a 5.6% increase from the RT value of U/W = 0.89, although this is not sufficiently accurate because reliable data of crystal structures below 100 K are presently available only for salts **d**, **e**, and **g**.

The on-site Coulomb repulsion energy U has an effect of enhancing spin susceptibility because the magnetic susceptibility is described as $\chi_{RT} = \chi_0/(1 - D(\varepsilon_F)U) = \chi_0/(1 - \xi)$, where χ_{RT} and χ_0 are the susceptibility at RT and the non-interacting susceptibility, respectively, and $D(\varepsilon_F)$ and ξ are density of state at Fermi level and the Stoner factor, respectively. In addition to the effect of U, the measured susceptibility is noticeably affected by the spin frustration t'/t.

Five κ-$(ET)_2X$ salts (**a**–**d**, **f**) have U/W values less than 0.89 at RT. These salts also have nearly the same EPR magnetic susceptibility at RT ($\chi_{RT} = 4.0 \times 10^{-4}$ to 5.5×10^{-4} emu/mol, as shown in Table 1 and Fig. 5b), with the exception of **a**, the data for which are not reported, which indicates a slightly large Stoner factor compared to that of the good metal (β-$(ET)_2AuI_2$ 3.4×10^{-4} emu/mol).[38b] Interestingly, the χ_{RT} of Mott insulator **e** was not different from those of **b**–**d** and **f**, and furthermore, above 100 K, they all behaved similarly both in magnitude and in the temperature dependence of χ.[24] These χ_{spin} data indicate that salts **b**–**f** have a very similar electronic structure above 100 K in good accordance with the temperature dependence of U/W for these salts above 100 K in Fig. 6.

Even though the χ_{RT} of the QSL system **g** (5.5×10^{-4} emu/mol) is not much different from those of the other κ-type salts listed in Table 1, all these values are distinctly lower than those of typical Mott insulators α'-$(ET)_2X$ (where X = $CuCl_2$, $AuBr_2$, $Ag(CN)_2$, 2-alkoxy-1,1,3,3-tetracyanoallyl (Fig. S1) and so on, many of which have unknown ground state)[43] and β'-$(ET)_2X$ (for X = ICl_2, IBrCl, and $AuCl_2$, all of which have AF ground state), where $\chi_{RT} = 9.0 \times 10^{-4}$ to 12×10^{-4} emu/mol.[44,45]

The presented transport data, magnetic data, and band parameters U/W above 100 K indicate that the salts $Ag(CN)_2 \cdot H_2O$ (**b**), Cu(CN)[$N(CN)_2$] (**c**), Cu[$N(CN)_2$]Br (**d**), $Cu(NCS)_2$ (**f**), Cu[$N(CN)_2$]Cl (**e**) and $Cu_2(CN)_3$ (**g**) are very close to the Mott boundary, in the metallic region for the former four salts whereas in the Mott insulating region for the latter two salts.

The effect of the spin frustration t'/t on χ is clearly seen for the Mott insulators **e** and **g** shown in Fig. 5b in the low temperature region. The χ of the AF system (**e**) vanishes at T_N, while that of the QSL system (**g**) exhibits an enhancement below 100 K with a maximum at around 20–30 K followed by a decrease with a nonzero value at 0 K. From this viewpoint, it is of great interest to know the range of t'/t values for the QSL state.

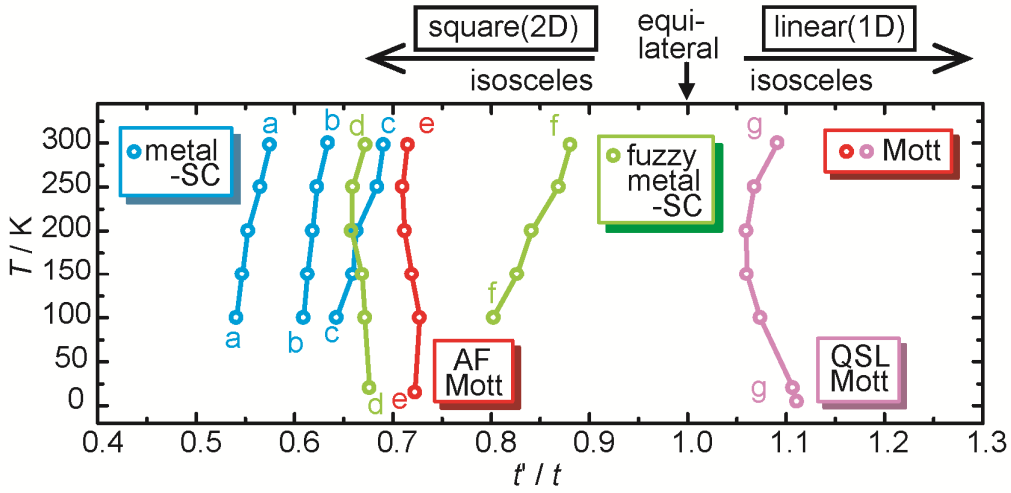

Fig. 7. Temperature dependence of t'/t of κ-$(ET)_2X$, where X = **a**: I_3, **b**: $Ag(CN)_2 \cdot H_2O$, **c**: Cu(CN)[$N(CN)_2$], **d**: Cu[$N(CN)_2$]Br, **e**: Cu[$N(CN)_2$]Cl, **f**: $Cu(NCS)_2$, and **g**: $Cu_2(CN)_3$. The color scheme employed is blue symbols: good metal, green symbols: fuzzy metal, red symbols: AF Mott insulator, and magenta symbols: QSL Mott insulator. The data below 100 K were calculated using the crystal structures measured by other laboratories (**d**,[39] **e**,[40] and **g**[41]).

Figure 7 shows the temperature dependence of t'/t of κ-$(ET)_2X$ calculated based on the crystal structures at different temperatures. The changes of t and t' differ from salt to salt (−6.5% (**f**) ~ +8.5% (**b**) from RT to 100 K). The t'/t values decreased by 5.9% for system **a**, 6.8% for **c**, and 8.7% for **f** from RT to 100 K. For the salts **a**–**c**, and **f**, the values of t'/t deviate from unity with decreasing temperatures down to 100 K, indicating that their spin frustration is weakened and approaches that of a 2D square spin lattice, whereas the t'/t values are nearly constant within small fluctuations to 100 K for the Mott insulators **e** and **g**. Therefore, the spin lattice geometries of nearly equilateral triangles for κ-$(ET)_2Cu_2(CN)_3$ and of isosceles triangles for κ-$(ET)_2Cu[N(CN)_2]Cl$ were retained at low temperatures in the QSL and AF states, respectively. Below 100 K, the t'/t values of **d** and **g** demonstrated a slight increase, showing a diversity of the temperature dependence of t'/t even in the κ-$(ET)_2X$ family. Figure 7 indicates that the QSL system **g** is allocated within the region $t'/t > 0.9$ (i.e., representing an equilateral triangle ~ linear spin lattice).

2-4. Design of QSL next to a Superconducting state

The electronic states of the dimerized ET salts including β-, β'-, κ-$(ET)_2X$, and the Mott insulator ET·TCNQ,[46] where TCNQ is tetracyanoquinodimethane, at high temperatures are roughly discriminated by the plot of W/U vs. W at RT shown in Fig. 8, and the information contained in the figure indicates the following points.

1) The values for W and W/U cover the ranges 0.25–0.61 eV and 0.47–1.25, respectively, for these salts, and a nearly linear relation exists between W/U and W.
2) Good metals **a**, **b**, **c**, **h**, **i**, and **j**, referred to in the figure by blue symbols, reside at the upper-right corner toward the itinerant region, though β-$(ET)_2AuI_2$ (**h**) has a somewhat smaller W/U due to a rather large U value (0.50 eV). The good metals have a rather low T_c less than 10 K (except for **c** with a T_c = 11.2 K).
3) Fuzzy metals **d** and **f**, given by green symbols, reside above the Mott insulators and among good metals with W/U in the range 1.1–1.2, and have a $T_c > 10$ K.
4) Dimer-type Mott insulators, given by the red triangles, are allocated inside the area depicted by the gray solid lines ($W/U < 1.12$ and $W < 0.57$ eV). The gray solid lines indicate the boundary between Mott insulating and itinerant regions.
5) Mott insulators **e** and **g** having W/U close to unity are converted to a metal or a superconductor by a slight pressure. A Mott insulator convertible to a metal or a superconductor under a slight pressure can be classified as a "soft" Mott insulator. These insulators are allocated near or inside the itinerant region with W/U and W values above the dotted gray lines, and they have rather small activation energies for conduction compared to those of the Mott insulators discussed in the following point ($\varepsilon_a > 0.11$ eV).
6) Typical Mott insulators **l** (T_N = 22 K),[44] **m** (T_N = 19.5 K),[45] and **n** (T_N = 28 K)[44] reside at the lower-left corner in the Mott region. Some of these become superconductors under extremely high pressure with a rather high T_c (8.2 GPa, onset T_c = 14.2 K for **l**, 8.0 GPa, onset T_c = 7.2 K for **m**).[45,47] Mott insulators, which are distantly located from the itinerant region and are not readily converted to a metal or superconductor, exhibit different transport and magnetic properties from those of "soft" Mott insulators, as mentioned above, and are denoted as "hard" Mott insulators.

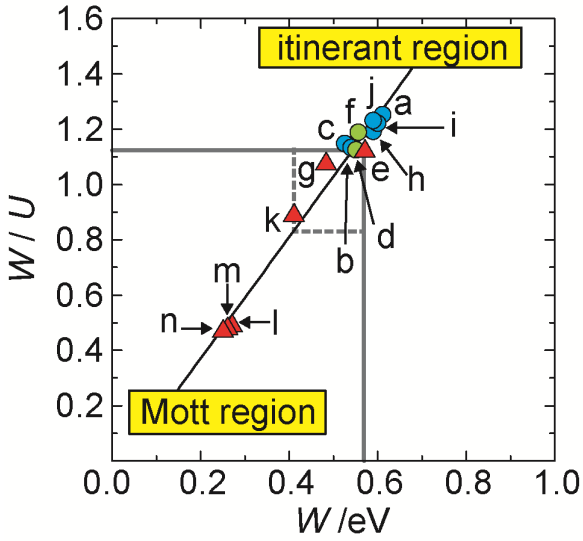

Fig. 8. The relation between W/U and bandwidth W for various ET compounds having dimerized ET molecules, given as (**a**) κ-$(ET)_2I_3$, (**b**) κ-$(ET)_2Ag(CN)_2{\cdot}H_2O$, (**c**) κ-$(ET)_2Cu(CN)[N(CN)_2]$, (**d**) κ-$(ET)_2Cu[N(CN)_2]Br$, (**e**) κ-$(ET)_2Cu[N(CN)_2]Cl$, (**f**) κ-$(ET)_2Cu(NCS)_2$, (**g**) κ-$(ET)_2Cu_2(CN)_3$, (**h**) β-$(ET)_2AuI_2$ (W = 0.59 and W/U = 1.19), (**i**) β-$(ET)_2IBr_2$ (W = 0.60 and W/U = 1.22), (**j**) β-$(ET)_2I_3$ (W = 0.59 and W/U = 1.23), (**k**) ET·TCNQ (triclinic, W = 0.41, and W/U = 0.89), (**l**) β'-$(ET)_2ICl_2$ (W = 0.27 and W/U = 0.49), (**m**) β'-$(ET)_2BrICl$ (W = 0.26 and W/U = 0.48), and (**n**) β'-$(ET)_2AuCl_2$ (W = 0.25 and W/U = 0.47) ● : representing good metals (**a**, **b**, **c**, **h**, **i**, and **j**); ● : representing fuzzy metals (**d** and **f**), and ▲ : representing dimer-type Mott insulators (**e**, **g**, **k**, **l**, **m**, and **n**) are allocated inside the area depicted by the gray solid lines. Those above the gray dotted lines are close to the itinerant region, and some of these are easily converted to a metal or a superconductor.

It is emphasized that the spins in κ-$(ET)_2X$ salts are subject to competition among localization, itinerancy, and frustration depending on the parameters U, W, t', and t. The competition between itinerancy (metal, superconductor), localization (Mott insulator), and frustration (AF, QSL) was theoretically discussed using a plot of U/t vs. t'/t values at 0 K by several groups.[48] Here our experimental results are presented on a U/W vs. t'/t plot (Fig. 9), since the contribution of t' in U/t at large t'/t becomes negligible, using the band parameters at 100 K (Table 1 for **a** – **g**, wherein data for **l** and **n** are at RT). At present, the phase boundaries depicted by the dotted lines in Fig. 9 are arbitrary.

Even though the AF salt **e** is on the boundary between the AF phase and the metal and superconductor region, the addition of two β'-type dimer Mott insulators (β'-$(ET)_2X$, for X = ICl_2 (**p**) and $AuCl_2$ (**r**)) reinforces the validity of the AF region at low t'/t and high U/W. The metal and superconducting salts are allocated below U/W = 0.9 and in the t'/t of 0.55–0.80 range. Since the metallic κ-$(ET)_2X$ so far prepared covers a limited t'/t range, we are not able to decide t'/t boundary for metal and superconductor region. The salt **g** resides at higher U/W and t'/t than those of salts in the metal and superconductor region. Here also we are not able to decide the exact boundary between AF and QSL Mott regions. This phase diagram is in good accordance with the facts that 1) the salt **e** becomes a metal and a superconductor under very weak pressure, 2) the salt **g** needs higher pressure to become a metal and a superconductor than that needed for **e**. Theoretically expected superconducting state near the QSL state was predicted to be d-symmetry.[48] In accordance with this, the superconducting symmetry of the salts **d**,[49] **f**,[50,51] and **g**[12] has been experimentally confirmed as d-wave.

However, the following information and studies are presently required to validate and improve the phase diagram and obtain a more effective materials design: 1) investigation of the parameters U/W and t'/t based on the crystal structures at lower temperatures for all salts, 2) development of metallic dimer-type ET salts having triangular spin lattices in the wide range of t'/t, 3) determination of the superconducting symmetry of materials that exhibit superconductivity, especially salts **a**–**c**, 4) search for QSL, AF, and/or superconducting states in the salts **e** and **f**, which are allocated near the phase boundaries, by changing the topological shape of the triangular spin lattice using the uniaxial strain method, and 5) search for new QSL systems using Figs. 5−9. For 4) and 5), the chemical modification of the polyanions that have given the κ-type ET arrangement would open up the unexplored region in Fig. 9, because the present study revealed that the anion structure is closely related to the electronic state of κ-$(ET)_2X$. Material exploration along this line, for example, by replacing the Cu(I) with a larger Ag(I) which may lead to even more-localized κ-$(ET)_2X$ salts (larger U/W), is in progress.

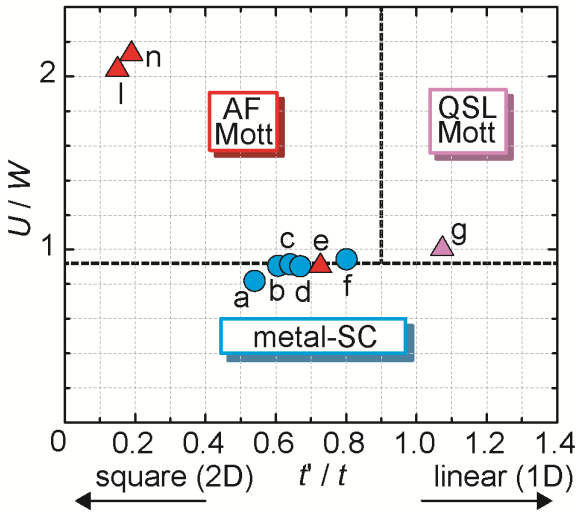

Fig. 9. Ground states of the dimerized ET salts (κ-$(ET)_2X$ listed in Table 1 and β'-$(ET)_2X$ (for X = ICl_2(**l**) and $AuCl_2$(**n**)) are plotted using U/W and t'/t. The following symbols are employed ●: metal-superconductor (SC), ▲: Mott insulator-AF, and △: Mott insulator-QSL. The band parameters of **a**–**g** are those listed in Table 1 at 100 K and the others are at RT. The salts are identified as (**a**) κ-$(ET)_2I_3$, (**b**) κ-$(ET)_2Ag(CN)_2{\cdot}H_2O$, (**c**) κ-$(ET)_2Cu(CN)[N(CN)_2]$, (**d**) κ-$(ET)_2Cu[N(CN)_2]Br$, (**e**) κ-$(ET)_2Cu[N(CN)_2]Cl$, (**f**) κ-$(ET)_2Cu(NCS)_2$, (**g**) κ-$(ET)_2Cu_2(CN)_3$, (**l**) β'-$(ET)_2ICl_2$ (t'/t = 0.15 and U/W = 2.04), and (**n**) β'-$(ET)_2AuCl_2$ (t'/t = 0.19 and U/W = 2.13).

We have demonstrated the 2D QSL system of the dimer-type Mott insulator together with metallic, superconducting, and AF solids of κ-$(ET)_2X$. Based on the crystal and band structures and physical properties, the following requirements are presently derived as designing principles for QSL systems next to a metal and superconductor state.

1) Low spin state (S = 1/2).
2) The system should be a Mott insulator having W < 0.57 eV and U/W > 0.89 at RT and U/W > 0.94 at low temperatures for κ-$(ET)_2X$.
3) The material's Mott insulating state has a partial CT state close to the itinerant region and a small Mott gap.

4) The spin lattice should have a geometry that affords a strong topological frustration of $t'/t > 0.9$ for a triangular spin lattice.
5) A high $|\Theta_{CW}|$ or high $|J|$ value is needed to observe the QSL state at experimentally available temperatures.
6) The material must maintain weak energy dispersion along the weakest direction for the magnetic interactions of the 2D system.

3. Conclusion

Geometrical spin frustration was discussed based on the key-keyhole relation for dimer-type Mott insulators of ET CT solids. Competition among the localization and the itinerancy of electrons, spin frustration, and unconventional spin pairing for superconductivity are the characteristic features of the dimer-type ET conductors. The key-keyhole relation of κ-$(ET)_2X$, representative of an ET dimer corresponding to one spin site positioned on an anion opening, provides for the QSL system κ-$(ET)_2Cu_2(CN)_3$ (t'/t = 1.09, U/W = 0.93, and $|J|$ = ~250 K), and some characteristic properties were described. The anion opening of κ-$(ET)_2Cu_2(CN)_3$ has a hexagonal shape, and ET dimers are positioned on each anion opening. κ-$(ET)_2Cu_2(CN)_3$ demonstrated an anisotropic superconducting state near the QSL state under pressure. Crystal design for the QSL system was discussed from the perspective of dimer-type ET Mott insulators using the key-keyhole relation and band parameters t, t', U, and W, namely $U/W > 0.89$, $t'/t > 0.90$, and $W < 0.57$ eV at RT and $U/W > 0.94$ at low temperatures.

To realize a QSL state next to a metal and a superconductor state, the system should satisfy 1) low-spin state, 2) Mott insulating state close to the itinerant region with a small Mott gap, 3) topologically strong spin frustration based on a spin geometry t'/t ~1 for a triangular spin lattice, and 4) a high $|\Theta_{CW}|$ value so as to observe the QSL state experimentally.

Experimental

The single crystals of κ-$(ET)_2X$ used in this study were prepared by the electrooxidation of ET in the presence of appropriate supporting electrolytes. Among these, the following notes should be mentioned. As for κ-$(ET)_2I_3$ (**a**), Balthes et al. reported that pure single crystals of κ-$(ET)_2I_3$ were prepared using $(TBA)I_3$, where TBA is tetrabutylammonium, as a supporting electrolyte;[52] however, only crystals of β-$(ET)_2I_3$ were obtained under this condition in our laboratory. Therefore, single crystals of κ-$(ET)_2I_3$ were obtained using a mixed supporting electrolyte of $(TBA)I_3$ and $(TBA)AuI_2$, as reported in ref. 22, and might therefore contain AuI_2 in the anion layer, which may inhibit the material's intrinsic physical properties. Our CT crystals of ET used in this study have identical structural data as those reported in the literature.

Single-crystal X-ray diffraction data were collected on a CCD-type diffractometer (Bruker SMART APEX II) with a graphite-monochromated Mo Kα radiation (λ = 0.71073 Å). The crystal structures were solved by a direct method using SHELXS[53] and were refined by a full-matrix least-squares method on F^2 using SHELXL.[53] The positional parameters of the hydrogen atoms were calculated at a fixed C–H bond length of 1.00 Å with sp^3 configuration of the bonding carbon atoms. CCDC 1016190 (100 K), 1016191 (150 K), 1016192 (200 K), 1016193 (250 K), and 1016194 (298 K) for κ-$(ET)_2I_3$, CCDC 1016290 (100 K), 1016291 (150 K), 1016292 (200 K), 1016293 (250 K), and 1016294 (300 K) for κ-$(ET)_2Ag(CN)_2 \cdot H_2O$,

CCDC 1016170 (100 K), 1016171 (150 K), 1016172 (200 K), 1016173 (250 K), and 1016174 (298 K) for κ-$(ET)_2Cu(CN)[N(CN)_2]$, CCDC 1016180 (100 K), 1016181 (150 K), 1016182 (200 K), 1016183 (250 K), and 1016184 (298 K) for κ-$(ET)_2Cu[N(CN)_2]Br$, CCDC 1016185 (100 K), 1016186 (150 K), 1016187 (200 K), 1016188 (250 K), and 1016189 (298 K) for κ-$(ET)_2Cu[N(CN)_2]Cl$, CCDC 1016175 (100 K), 1016176 (150 K), 1016177 (200 K), 1016178 (250 K), and 1016179 (298 K) for κ-$(ET)_2Cu(NCS)_2$, CCDC 1016295 (100 K), 1016296 (150 K), 1016297 (200 K), 1016298 (250 K), and 1016299 (300 K) for κ-$(ET)_2Cu_2(CN)_3$ are contained in the supplementary crystallographic data of this paper. These data can be obtained free of charge from The Cambridge Crystallographic Data Centre via www.ccdc.cam.ac.uk/data_request/cif.

The transfer integrals (t) between ET molecules were calculated within a tight-binding approximation, using the extended Hückel molecular orbital method with single-ζ parameters including d-orbitals of sulfur atoms based on the observed crystal structures.[29] The HOMO of the molecule was used as the basis function. Semi-empirical parameters for Slater-type atomic orbitals were used. The t values were assumed to be proportional to the overlap integral (S) via the equation $t = ES$ ($E = -10$ eV).

Acknowledgments

This study was supported by Grant-in-Aid Scientific Research from JSPS, Japan (23225005) "Development of multi-electronic-functions based on spin triangular lattice."

References

1 a) D. Huse, V. Eser, *Phys. Rev. Lett*., 1988, **60**, 2531–2534.
b) J. E. Greedan, *J. Mater. Chem*., 2001, **11**, 37–53.
2 a) P. W. Anderson, *Mater. Res. Bull.,* 1973*,* **8**, 153–160.
b) P. Fazekas, P. W. Anderson, *Philos. Mag.*, 1974, **30**, 423–440.
3 G. H.Wannier, *Phys. Rev*., 1950, **79**, 357–364.
4 a) L. Balents, *Nature*, 2010, **464**, 199–208.
b) M. R. Norman, *Science*, 2011, **332**, 196–200.
5 a) A. Ramirez, *Annul. Rev. Mater. Sci.*, 1994, **24**, 453–480.
b) P. Schiffer, A. P. Ramirez, *Comments Condens. Matter Phys*., 1996, **18**, 21–50.
6 a) K. Hirakawa, H. Kadowaki, K. Ubukoshi, *J. Phys. Soc. Jpn.*, 1983, **52**, 1814–1824.
b) J. L. Manson, E. Ressouche, J. S. Miller, *Inorg. Chem.*, 2000, **39**, 1135–1141.
7 a) Y. Shimizu, K. Miyagawa, K. Kanoda, M. Maesato, G. Saito, *Phys. Rev. Lett.,* 2003, **91**, 107001/1–4.
b) S. Ohira, Y. Shimizu, K. Kanoda, G. Saito, *J. Low Temp. Phys*., 2006, **142**, 153–158.
c) F. L. Pratt, P. J. Baker, S. J. Blundell, T. Lancaster, S. Ohira-Kawamura, C. Baines, Y. Shimizu, K. Kanoda, I. Watanabe, G. Saito, *Nature,* 2011, **471**, 612–616.
8 N. F. Mott, in *Metal-Insulator Transitions*, Taylor and Francis, London, 2nd edn., 1990.
9 a) Y. Shimizu, M. Maesato, G. Saito, O. Drozdova, L. Ouahab, *Synth. Met.*, 2003, **133–134**, 225–226.
b) G. Saito, M. Maesato, *Mol. Cryst. Liq. Cryst.*, 2006, **455**, 31–46.
c) Y. Shimizu, M. Maesato, G. Saito, *J. Phys. Soc. Jpn.*, 2011, **80**, 074702/1–7.
10 C. W. Chu, *Nature Phys.*, 2009, **5**, 787–789.
11 Y. Iwasa, T. Takenobu, *J. Phys.: Condens. Matter*, 2003, **15**, R495–R519.
12 Y. Shimizu, H. Kasahara, T. Furuta, K. Miyagawa, K. Kanoda, M. Maesato, G. Saito, *Phys. Rev. B*, 2010, **81**, 224508/1–4.
13 a) G. Saito, Y. Yoshida, *Bull. Chem. Soc. Jpn.*, 2007, **80**, 1–137.
b) G. Saito, Y. Yoshida, *Chem. Record*, 2011, **11**, 124–145.
14 B. J. Powell, R. H. McKenzie, *Rep. Prog. Phys.*, 2011, **74**, 056501/1–60.
15 T. Isono, H. Kamo, A. Ueda, K. Takahashi, M. Kimata, H. Tajima, S. Tsuchiya, T. Terashima, S. Uji, H. Mori, *Phys. Rev. Lett.*, 2014, **112**, 177201/1–5.
16 a) T. Itou, A. Oyamada, S. Maegawa, M. Tamura, R. Kato, *J. Phys.: Condens. Matter,* 2007, **19**, 145247/1–5.
b) T. Itou, A. Oyamada, S. Maegawa, M. Tamura, R. Kato, *Phys. Rev. B*, 2008, **77**, 104413/1-5.

17 T. -H. Han, J. S. Helton, S. Chu, D. G. Nocera, J. A. Rodriguez-Rivera, C. Broholm, Y. S. Lee, *Nature*, 2012, **492**, 406–410.
18 Y. Okamoto, M. Nohara, H. Aruga-Katori, H. Takagi, *Phys. Rev. Lett*., 2007, **99**, 137207/1–4.
19 a) K. Hirakawa, H. Kadowaki, K. Ubukoshi, *J. Phys. Soc. Jpn*., 1985, **54**, 3526–3535.
b) S. J. Clarke, A. J. Fowkes, A. Harrison, R. M. Ibberson, M. J. Rosseinsky, *Chem. Mater*., 1998, **10**, 372–384.
20 a) S. Nakatsuji, Y. Nambu, H. Tonomura, O. Sakai, C. Broholm, H. Tsunetsugu, Y. Qiu, Y. Maeno, *Science*, 2005, **309**, 1697–1700.
b) S. Nakatsuji, Y. Nambu, K. Onuma, S. Jonas, C. Broholm, Y. Maeno, *J. Phys.: Condens. Matter*, 2007, **19**, 145232/1–7.
21 a) Z. Hiroi, N. Kobayashi, M. Hanawa, M. Nohara, H. Takagi, Y. Kato, M. Takigawa, *J. Phys. Soc. Jpn*., 2001, **70**, 3377–3384.
b) H. Yoshida, Y. Okamoto, T. Tayama, T. Sakakibara, M. Tikunaga, A. Matsuo, Y. Narumi, K. Kindo, M. Yoshida, M. Takigawa, Z. Hiroi, *J. Phys. Soc. Jpn*., 2009, **78**, 043704/1–4.
22 a) A. Kobayashi, R. Kato, H. Kobayashi, S. Moriyama, Y. Nishio, K. Kajita, W. Sasaki, *Chem. Lett*., 1987, 459–462.
b) R. Kato, H. Kobayashi, A. Kobayashi, S. Moriyama, Y. Nishio, K. Kajita, W. Sasaki, *Chem. Lett*., 1987, 507–510.
23 H. Mori, I. Hirabayashi, S. Tanaka, T. Mori, H. Inokuchi, *Solid State Commun*., 1990, **76**, 35–37.
24 T. Nakamura, T. Nobutoki, T. Takahashi, G. Saito, H. Mori, T. Mori, *J. Phys. Soc. Jpn.*, 1994, **63**, 4110–4125.
25 M. Kini, U. Geiser, H. H. Wang, K. D. Carlson, J. M. Williams, W. K. Kwok, K. G. Vandervoort, J. E. Thompson, D. L. Stupka, D. Jung, M. -H. Whangbo, *Inorg. Chem.*, 1990, **29**, 2555–2557.
26 J. M. Williams, A. M. Kini, H. H. Wang, K. D. Carlson, U. Geiser, L. K. Montgomery, G. J. Pyrka, D. M. Watkins, J. M. Kommers, S. J. Boryschuk, A. V. Crouch, W. K. Kwok, J. E. Schirber, D. L. Overmyer, D. Jung, M. -H. Whangbo, *Inorg. Chem.*, 1990, **29**, 3272–3274.
27 a) U. Welp, S. Fleshler, W. K. Kwok, G. W. Crabtree, K. D. Carlson, H. H. Wang, U. Geiser, J. M. Williams, V. M. Hitsman, *Phys. Rev. Lett*., 1992, **69**, 840–843.
b) K. Miyagawa, K. Kawamoto, Y. Nakazawa, K. Kanoda, *Phys. Rev. Lett*., 1995, **75**, 1174–1177.
28 a) A. B. Harris, R. V. Lange, *Phys. Rev.*, 1967, **157**, 295–314.
b) M. Tamura, R. Kato, *J. Phys. Soc. Jpn.*, 2004, **73**, 3108–3110.
29 T. Mori, A. Kobayashi, Y. Sasaki, H. Kobayashi, G. Saito, H. Inokuchi, *Bull. Chem. Soc. Jpn.*, 1984, **57**, 627–633.
30 a) U. Geiser, H. H. Wang, K. D. Carlson, J. M. Williams, H. A. Charlier Jr., J. E. Heindl, G. A. Yaconi, B. H. Love, M. W. Lathrop, J. E. Schirber, D. L. Overmyer, J. Ren, M. -H. Whangbo, *Inorg. Chem.*,1991, **30**, 2586–2588.
b) T. Komatsu, T. Nakamura, N. Matsukawa, H. Yamochi, G. Saito, *Solid State Commun.*, 1991, **80**, 843–847.
c) H. Yamochi, T. Nakamura, T. Komatsu, N. Matsukawa, T. Inoue, G. Saito, T. Mori, M. Kusunoki, K. Sakaguchi, *Solid State Commun*., 1992, **82**, 101–105.
d) T. Komatsu, N. Matsukawa, T. Inoue, G. Saito, *J. Phys. Soc. Jpn.*, 1996, **65**, 1340–1354.
31 a) E. Ohmichi, H. Ito, T. Ishiguro, T. Komatsu, G. Saito, *J. Phys. Soc. Jpn.*, 1997, **66**, 310–313.
b) E. Ohmichi, H. Ito, T. Ishiguro, G. Saito, *Phys. Rev. B*., 1998, **57**, 7481–7484.
32 General:
a) T. Ishiguro, K. Yamaji, G. Saito, in *Organic Superconductors*, Springer-Verlag, Berlin, 2nd edn., 1998, Appendix, pp. 455–458.
b) J. Wosnitza, in *Fermi Surfaces of Low-Dimensional Organic Metals and Superconductors*, Springer-Verlag, Berlin, 1996.
c) J. Singleton, *Rep. Prog. Phys*., 2000, **63**, 1111–1207.
33 H. Yamochi, T. Komatsu, N. Matsukawa, G. Saito, T. Mori, M. Kusunoki, K. Sakaguchi, *J. Am. Chem. Soc.,*1993, **115**,11319–11327.
34 a) H. Urayama, H. Yamochi, G. Saito, K. Nozawa, T. Sugano, M. Kinoshita, S. Sato, K. Oshima, A. Kawamoto, J. Tanaka, *Chem. Lett*., 1988, 55–58.
b) H. Urayama, H. Yamochi, G. Saito, S. Sato, A. Kawamoto, J. Tanaka, T. Mori, Y. Maruyama, H. Inokuchi, Chem. Lett., 1988, 463–466.
35 a) U. Geiser, H. H. Wang, L. E. Gerdom, M. A. Firestone, L. M. Sowa, J. M. Williams, *J. Am. Chem. Soc*., 1985, **107**, 8305–8307.
b) U.Geiser, H. H. Wang, J. M. Williams, E. L. Venturini, J. F. Kwak, M.-H. Whangbo, *Synth. Met.*, 1987, **19**, 599–604. They suggested metallic nature based on the band calculation and EPR measurements. However, we have confirmed the AF transition by ^{1}H NMR measurements. c) T.

Hiramatsu, Y. Yoshida, G. Saito, Y. Shimizu, M. Maesato, A. Otsuka, Y. Yamochi, presented in part at the 94 th Spring Meeting of Chemical Society of Japan, 1D3-34A, Nagoya, Japan, March, 2014.

36 a) S. Golhen, L. Ouahab, A. Lebeuze, M. Bouayed, P. Delhaes, Y. Kashimura, R. Kato, L. Binet, J.-M. Fabre, *J. Mater. Chem.*, 1999, **9**, 387–393.
b) S. V. Ivanov, S. M. Miller, O. P. Anderson, S. H. Strauss, *Cryst. Growth Des.*, 2004, **4**, 249–254.
Accordingly we have prepared new QSL system using Ag^{+} (κ-$(ET)_2Ag_2(CN)_3$), which has triangular spin lattice (t'/t = 0.97, U/W = 1.04); c) G. Saito, Y. Yoshida, T. Hiramatsu, A. Otsuka, M. Maesato, Y. Shimizu, H. Ito, H. Kishida, presented in part at the 10th International Symposium of Crystalline Organic Metal, Superconductors, Ferromagnets, Montreal, Canada, July, 2013. d) T. Hiramatsu, Y. Shimizu, M. Maesato, A. Otsuka, H. Yamochi, Y. Yoshida. G. Saito, presented in the 7th Annual Meeting of Japan Society for Molecular Science, 1B-05, Kyoto, Japan, September, 2013. e) Y. Shimizu, T. Hiramatsu, Y. Yoshida, M. Maesato, A. Otsuka, H. Yamochi, G. Saito, presented in part at Fall Meeting of the Physical Society of Japan, 28aDJ-1, Tokushima, Japan, September, 2013. f) M. Maeasto, T. Hiramatsu, Y. Yoshida, G. Saito, H. Kitagawa, presented in part at Fall Meeting of the Physical Society of Japan, 28aDJ-2, Tokushima, Japan, September, 2013. g) Y. Nakamura, H. Kishida, T. Hiramatsu, Y. Yoshida, G. Saito, presented in the 69th Annual Meeting of the Physical Society of Japan, 30aCL-6, Hiratsuka, Japan, March, 2014. h) Y. Shimizu, T. Hiramatsu, M. Maesato, A. Otsuka, M. Yoshida, M. Takigawa, A. Ono, M. Itoh, H. Yamochi, Y. Yoshida, G. Saito, unpublished work.

37 E. S. Gruff, S. A. Koch, *J. Am. Chem. Soc.*, 1989, **111**, 8762–8763.

38 a) H. H. Wang, L. Nunez, G. W. Carlson, J. M. Williams, J. L. Azevedo, J. F. Kwak, J. E. Schirber, *Inorg. Chem.*, 1985, **24**, 2465–2466.
b) D. R. Talham, M. Kurmoo, P. Day, D. S. Obertelli, I. D. Parker, R. H. Friend, *J. Phys.*, 1986, **C19**, 383–388.

39 U. Geiser, A. M. Kini, H. H. Wang, M. A. Beno, J. M. Williams, *Acta Cryst.*, 1991, **C47**, 190–192.

40 M. Watanabe, Y. Nogami, K. Oshima, H. Ito, T. Ishiguro, G. Saito, *Synth. Met.*, 1999, **103**, 1909–1910.

41 H. O. Jeschke, M. de Souza, R. Valenti, R. S. Manna, M. Lang, J. A. Schlueter, *Phys. Rev. B*, 2012, **85**, 035125/1–7.

42 a) K. Kanoda, *Hyperfine Interact.*, 1997, **104**, 235–249.
b) K. Kanoda, *J. Phys. Soc. Jpn.*, 2006, **75**, 051007/1–16.

43 a) S. D. Obertelli, R. H. Friend, D. R. Talham, M. Kurmoo, P. Day, *J. Phys.: Condens. Matter*, 1989, **1**, 5671–5680.
b) S. Sekizaki, H. Yamochi, G. Saito, *Synth. Met.*, 2001, **120**, 961–962.

44 N. Yoneyama, A. Miyazaki, T. Enoki, G. Saito, *Bull. Chem. Soc. Jpn.*, 1999, **72**, 639–651.

45 K. Uchiyama, M. Miyashita, H. Taniguchi, K. Satoh, N. Mori, K. Miyagawa, K. Kanoda, M. Hedo, Y. Uwatoko, *J. Phys. IV*, 2004, **114**, 387–389.

46 Y. Iwasa, K. Mizuhashi, T. Koda, Y. Tokura, G. Saito, *Phys. Rev. B*, 1994, **49**, 3580–3583.

47 H. Taniguchi, M. Miyashita, K. Uchiyama, K. Satoh, N. Mori, H. Okamoto, K. Miyagawa, K. Kanoda, M. Hedo, Y. Uwatoko, *J. Phys. Soc. Jpn.*, 2003, **72**, 468–471.

48 a) H. Morita, S. Watanabe, M. Imada, *J. Phys. Soc. Jpn.*, 2002, **71**, 2109–2112.
b) B. Kyung, A.-M. S. Tremblay, *Phys. Rev. Lett.*, 2006, **97**, 046402/1–4.
c) H. Shinaoka, T. Misawa, K. Nakamura, M. Imada, *J. Phys. Soc. Jpn.*, 2012, **81**, 034701/1-12.

49 K. Ichimura, M. Takami, K. Nomura, *J. Phys. Soc. Jpn.*, 2008, **77**, 114707/1–6.

50 T. Arai, K. Ichimura, K. Nomura, *Phys. Rev. B*, 2001, **63**, 104518/1–5.

51 K. Izawa, H. Yamaguchi, T. Sasaki, Y. Matsuda, *Phys. Rev. Lett.*, 2002, **88**, 27002/1–4.

52 E. Balthes, D. Schweitzer, I. Heinen, H. J. Keller, W. Strunz, W. Biberacher, A. G. M. Jansen, E. Steep, *Z. Phys. B*, 1996, **99**, 163–171.

53 G. M. Sheldrick, *Acta Cryst.,* 2008, **A64**, 112–122.

Table of contents entry

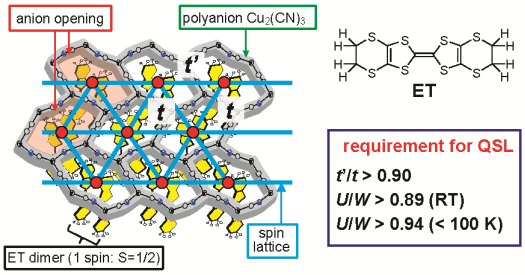

We propose the material design for quantum spin liquid next to super conducting state based on dimer-type ET Mott insulator.